Scientia Iranica D (2020) 27(6), 3150–3161

Sharif University of Technology
Scientia Iranica
Transactions D: Computer Science & Engineering and Electrical Engineering
http://scientiairanica.sharif.edu

Design modifications for improving modulation flux capability of consequent-pole vernier-PM machine in comparison to conventional vernier-PM machines

H. Gorginpour*

Department of Engineering, Persian Gulf University, Bushehr, P.O. Box 7516913817, Iran.

Received 24 July 2018; received in revised form 25 November 2018; accepted 7 January 2019

KEYWORDS
Consequent-pole Vernier-PM machine;
Flux modulation;
Flux density distribution;
Finite element method;
Spatial harmonics.

Abstract. The Vernier PM (VPM) machine is known as a high-torque and low-speed drive solution suitable for direct-drive applications such as electric vehicles and wind turbines. The Consequent-Pole VPM (CP-VPM) machine is a special structure of VPM that introduces high-torque density as the conventional VPM by incorporating the significantly lower volume of PM materials. Despite the large body of recent research and many experiments concerning the conventional structure, the CP-VPM machine has received attention only by few publications. The paper presented the electromagnetic principles of flux modulation in the CP-VPM machine. The quantities of machine operation were evaluated using analytical equations and the performance of the mentioned machine was compared with that of the conventional machine. It was concluded that the torque density and back EMF of the proposed machine were much larger than those of the conventional machine and the torque pulsation magnitude was lower. However, the power factor was undesirably reduced due to higher spatial harmonic distortion of the CP rotor magnetic field and the presence of magnetic field components, which would not contribute to the flux modulation. Based on the spatial harmonic analysis, design modifications made for enhancing the operational characteristics of the CP-VPM machine were proposed and their effectiveness was verified by comparing the 2D-FE results with those of the conventional VPM machines.

1. Introduction

PM machines have been widely utilized in several applications such as industrial servos, energy extraction from wind and other renewable energy resources, and electric transportation systems, especially over the past 20 years [1]. This popularity results from such advantages as high torque and power densities, desirable efficiency and power-factor, higher reliability, lower inertial, and simpler mechanical structure than other electric drive topologies [2]. The substantial improvements to the field of high energy density rare-earth permanent magnet materials pave the way for their widespread utilization in PM machines. However, the cost of these PM materials is still a significant portion of the overall machine manufacturing cost. Although the use of low-cost PM materials reduces the cost, the torque density diminishes severely [3].

Following the introduction of Vernier effect on the electromagnetic torque produced by reluctance motors, it was proposed that the mentioned effect be applied to magnetic gears [4]. The magnetic gear with Vernier principle was, in fact, the Vernier PM (VPM) machine introduced in 1995 [5]. This electric machine topology

*. *E-mail address: h_gorgin@pgu.ac.ir*

doi: 10.24200/sci.2019.51473.2198

has drawn considerable research interest lately. Recently, the consequent-pole PM machines have been introduced and investigated to improve the efficient use of PM materials [6]. The Consequent-Pole VPM (CP-VPM) is a special topology of VPM machines, requiring much lower volume of PM materials than the Conventional VPM (CVPM) structure with the same torque density. Besides, the reluctance torque developed due to the interaction of stator field and rotor teeth increases the torque density. Moreover, the magnet leakage flux and the cogging torque will be reduced using the CP type of VPM machine [7]. The basic structures of the CVPM and CP-VPM machines are given in Figure 1. According to Figure 1(a), the number of PM pieces installed on a VPM rotor is much larger than that of winding poles. This is the difference between a surface-mounted PM machine and a VPM machine.

The electromagnetic operating principle of the VPM machine is based on the flux modulation through the reaction between the spatial harmonics of the air-gap permeance, which are due to slotting effects, and the MMF of rotor PMs. This reaction is called the Vernier effect and results in higher back EMF and higher power density than the conventional PM machine. Several studies on the modeling, design, fabrication, geometrical optimization and introduction of new structures of radial flux, axial flux, and linear VPM machines have been reported, e.g., [8–14]. However, the operating principles of the CP-VPM machine and the comparison of its performance and other VPM structures have not been discussed in previous publications.

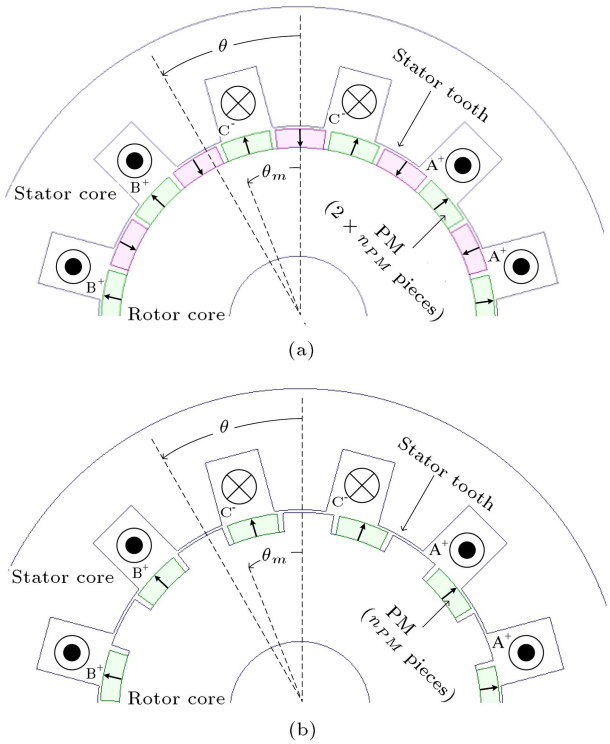

Figure 1. 2D cross-section geometrical view of (a) conventional VPM structure and (b) Consequent-Pole Vernier PM (CP-VPM) structure.

The aim of this paper is to investigate the flux modulation capability and the operating characteristics of the CP-VPM machine. Complicated distribution of air-gap flux density is analytically calculated and spatial harmonic components of the air-gap permeance function are determined. The effects of the design factors on the performance characteristics are predicted and design modifications are proposed for enhancing the air-gap flux density distribution and improving the performance quantities, especially the power factor. Finally, the effectiveness of the proposed geometric and design modifications is evaluated by comparing the performance of CVPM and CP-VPM machines.

2. Generic analysis of CP-VPM machine

The operation and design principles of the CVPM machine are studied in several pieces of literature and analytical equations which are supported by Finite Element (FE) and experimental results are derived for the torque, back EMF, power-factor, etc. The nature of VPM motor was analytically surveyed in [15] and also, the main geometric factors affecting power density and power factor were studied. The objective of [16] is to develop general design guidelines on different types of VPM machines based on the analytical relations of design parameters. The torque capability and quality of VPM machine were compared with those of regular PM machine in [17] and analytical expressions for average and ripple torques were derived using spatial harmonic analysis of air-gap permeance function. Also, the working principles of different topologies of CVPM machines based on the magnetic field modulation theory were discussed in [18–22].

In CVPM machine, the PM pieces are installed on the rotor surface with successively reversed polarizations. The number of PM pairs (n_{PM}) is determined based on the number of stator slots (N_{ss}) and the number of winding pole pairs (P) as follows:

$$n_{PM} = N_{ss} - P. \tag{1}$$

This is a well-known rule that brings about the phenomenon of flux modulation.

The number of PM pieces in CP topology is half of the total number of these pieces in a conventional PM Vernier rotor. Hence, the number of magnets is equal to that of rotor slots (N_{rs}). These magnets are inserted in between rotor teeth and they are characterized by the same magnetic polarization. The creation of successive N and S poles on the CP rotor can be explained

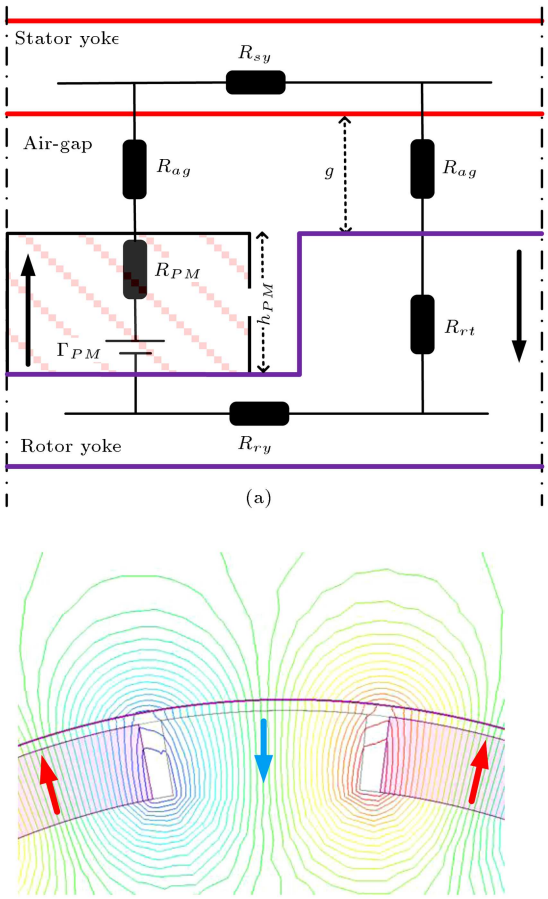

Figure 2. Creation of the S-poles in the CP rotor topology: (a) Magnetic equivalent circuit regardless of the leakage flux routes and stator slots and (b) 2D flux lines distribution of two PM pieces (N-pole) and their adjacent tooth (S-pole).

using magnetic circuits. Figure 2 shows the simplified magnetic circuits of the CP-VPM structure regardless of the leakage flux routes and stator slots. Γ_{PM} is the PM magneto-motive force (mmf), $\mathcal{R}_{PM}$ the PM reluctance, $\mathcal{R}_{ag}$ the air-gap reluctance, and $\mathcal{R}_{sy}$, $\mathcal{R}_{ry}$, and $\mathcal{R}_{rt}$ represent reluctances of the stator yoke, rotor yoke, and rotor tooth sections, respectively. Also, a 2D view of the flux lines is shown, coinciding with the flux tubes defined in the magnetic circuit. It can be seen that the tooth face is magnetized in the opposite direction of its adjacent PM pieces. In addition, the magnetic field magnitude of rotor tooth with S-polarization is lower than the flux density magnitude of PM section with N-polarization due to MMF drops.

The operating torque is created out of the interaction between P pole-pairs components of stator and rotor fields at a synchronous speed of $60 \times f_s/n_{PM}$, where f_s is the excitation frequency. The stator and rotor magnetic fields are obtained by multiplying their related MMF distributions and the air-gap permeance function. This function is the mathematical description of the variable air-gap length because of slotting effects. The air-gap permeance function due to the stator slotting and considering the slot-less rotor structure, i.e., CVPM configuration, can be written as Eq. (2) [23]:

$$\Lambda_s(\theta) = \Lambda_{s0} + \sum_{n=0}^{\infty} \Lambda_{sn} \cos(nN_{ss}\theta), \tag{2}$$

$$\Lambda_{s0} = \mu_0(1 - 1.6\beta w_{sso}/\tau_{ss})/g, \tag{3}$$

$$\beta = 0.5(1 - 1/\sqrt{[1 + (0.5w_{sso}/g)^2}), \tag{4}$$

$$\Lambda_{sn} = \mu_0\beta/g \times F_n(w_{sso}/\tau_{ss}), \tag{5}$$

$$F_n(w_{sso}/\tau_{ss}) = 2/(n\pi) \times 0.39/(0.39 - (w_{sso}/\tau_{ss})^2) \times \sin(1.6n\pi w_{sso}/\tau_{ss}), \tag{6}$$

where τ_{ss} is the stator slot pitch length.

The rotor permeance function in the case of CP-VPM is as Eq. (7):

$$\Lambda_r(\theta, \theta_m) = \Lambda_{r0} + \sum_{k=1}^{\infty} \Lambda_{rk} \cos(kN_{rs}(\theta - \theta_m)), \tag{7}$$

where Λ_{r0} and Λ_{rk} have the same relations as Eqs. (3) and (5), respectively, considering appropriate substitutions.

By using Eqs. (2) and (7), the air-gap permeance function of CP-VPM structure is obtained through Eq. (8):

$$\begin{aligned}\Lambda_{ag}(\theta, \theta_m) = \Lambda_{ag0} &+ \{\Lambda_{s1} cos(N_{ss}\theta)/k_{cr} \\ &+ \Lambda_{s2} cos(2N_{ss}\theta)/k_{cr} + ...\} \\ &+ \{\Lambda_{r1} cos(N_{rs}(\theta - \theta_m))/k_{cs} \\ &+ \Lambda_{r2} cos(2N_{rs}(\theta - \theta_m))/k_{cs} + ...\} \\ &+ \{g\Lambda_{s1}\Lambda_{r1} \times 0.5[\cos((N_{ss} + N_{rs})\theta - N_{rs}\theta_m) \\ &+ \cos((N_{ss} - N_{rs})\theta + N_{rs}\theta_m)] + ...\},\end{aligned} \tag{8}$$

$$\Lambda_{ag0} = \mu_0/(gk_{cs}k_{cr}), \tag{9}$$

where k_{cs} and k_{cr}, defined in Eq. (10), are the stator and rotor Carter's factors, respectively.

$$k_{cs/cr} = \tau_{ss/rs}/(\tau_{ss/rs} - 1.6\beta w_{sso/rso}). \tag{10}$$

The values of function F_n at different ratios of w_{sso}/τ_{ss} are plotted in Figure 3. Λ_{s0} determines the components of P-pole pairs of the stator rotating field, while those of P-pole pairs of the rotor field are created from the magnetic flux modulation of the N_{rs} pole-pair component of the rotor MMF function and Λ_{s1} term.

Table 1. The specifications of the studied CPM and Consequent-Pole Vernier PM (CP-VPM) structures.

Parameter	Symbol	Value
Number of stator slots	N_{ss}	12
Number of rotor slots	N_{rs}	0(CVPM), 11(CP-VPM)
Number of PM pieces	n_{PM}	22(CVPM), 11(CP-VPM)
Number of phases	m	3
Physical stack length	l_{fe}	65 mm
Stator outer diameter	D_{so}	120 mm
Stator inner diameter	D_{si}	75 mm
Stator slot opening width	w_{sso}	10 mm
Rotor outer radius	D_{ro}	74 mm
Rotor inner radius	D_{ri}	48 mm
Rotor slot opening width	w_{rso}	11.5 mm
Air-gap length	g	0.5 mm
PM thickness	h_{PM}	3.5 mm
PM arc-ratio	α_{PM}	0.45
PM remanence (20°C)	B_{r0}	1.1 T
PM relative permeability	μ_{PM}	1
PM conductivity	σ_{PM}	6.94×10^5 $(\Omega m)^{-1}$
Turns per coil	N_{sw}	200
Current	I_s	1.5 Arms
Rotational speed	n_m	272.73 rpm

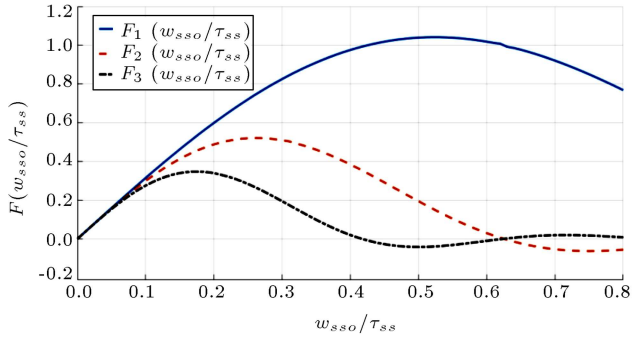

Figure 3. Plots of F_n function at different ratios of w_{sso}/τ_{ss}.

The air-gap permeance distribution has a much more complicated waveform in CP-VPM machine than the CVPM machine. The low-order spatial harmonic components of Λ_{ag} with the existing magnitudes for both studied topologies are depicted in Figure 4. The specifications of these structures are given in Table 1.

Using CP rotor, the average value and the Nss pole-pair component of the air-gap permeance are increased considerably because of the reduced effective air-gap length. Also, a P pole-pair term presented in Λ_{ag} develops the coupling of reluctance torque and the stator rotating field. However, the other harmonics are undesirable and result in increment of the differential leakage inductance.

The magnetic field of PMs is obtained analytically

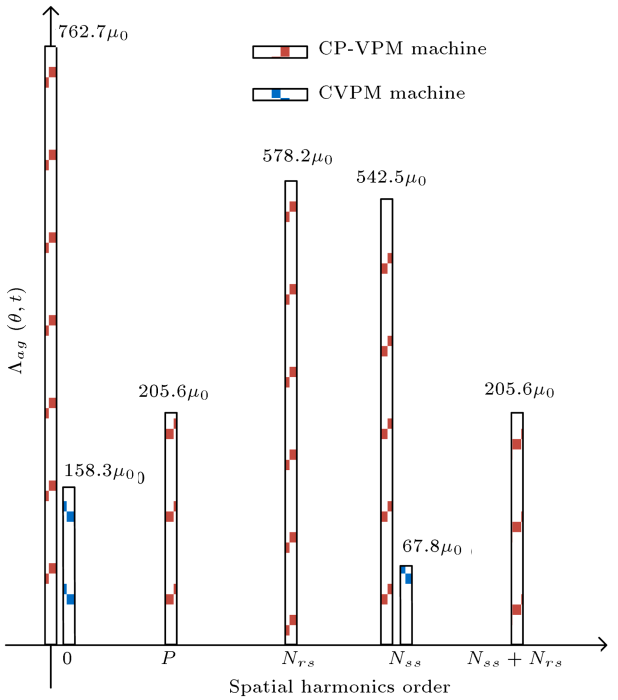

Figure 4. The dominant spatial harmonics of Λ_{ag} for the studied Conventional VPM (CVPM) and Consequent-Pole Vernier PM (CP-VPM) machines.

by multiplying PMs MMF and Λ_{ag} distributions. The MMF distributions of both rotor topologies over one pole pitch length are given in Figure 5. The MMF

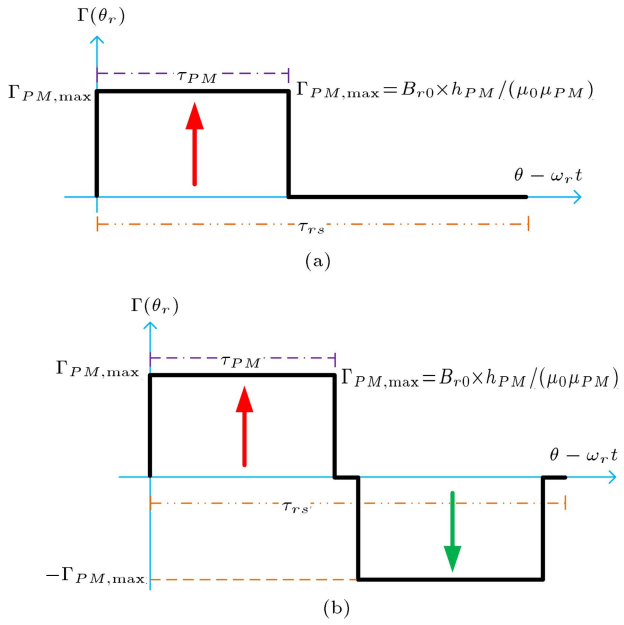

Figure 5. The MMF distribution over one pole pitch length of: (a) Consequent-Pole Vernier PM (CP-VPM) machine and (b) Conventional VPM (CVPM) machine.

function of CVPM rotor only contains odd harmonic components, while even components exist in the PM MMF of CP-VPM topology.

The air-gap magnetic field distributions due to parallel magnetized PMs and considering slot-less stator core are shown in Figure 6(a), which are obtained using 2D-FE analysis. These distributions are the radial components of the magnetic flux density vectors in the middle of air-gap regions of the studied machines. The tangential components of magnetic flux density vectors are compared, as shown in Figure 6(b). The dominant spatial harmonic components of these distributions are compared in Figure 6(c). The calculated values of these components are in good agreement with the FE results, e.g., the calculated values of B_{ag0} (1 pole-pair component) and B_{ag1} (11 pole-pairs component) of the studied CP-VPM machine are 0.43 T and 0.58 T, respectively.

The air-gap flux density distribution of a CP-VPM can be written as Eq. (11):

$$\begin{aligned} B(\theta,\theta_m) &= \Gamma_{PM}(\theta,\theta_m)\Lambda_{ag}(\theta,\theta_m) \\ &= B_{ag0}\cos(N_{rs}\omega_r t - N_{rs}\theta) + B_{ag1} \\ &\times\{\cos(N_{rs}\omega_r t + \overbrace{(N_{ss}-N_{rs})}^{P}\theta) \\ &+\cos(N_{rs}\omega_r t - (N_{ss}+N_{rs})\theta)\} \\ &+\Gamma_{PM1}\Lambda_{r1}/(2k_{cs})\times\cos(2N_{rs}(\omega_r t-\theta)) \\ &+\Gamma_{PM1}\Lambda_{s1}\Lambda_{r1}g/4\times\{\cos(2N_{rs}\omega_r t \\ &+(N_{ss}-2N_{rs})\theta)+\cos(2N_{rs}\omega_r t \\ &-(N_{ss}+2N_{rs})\theta)\}, \end{aligned} \tag{11}$$

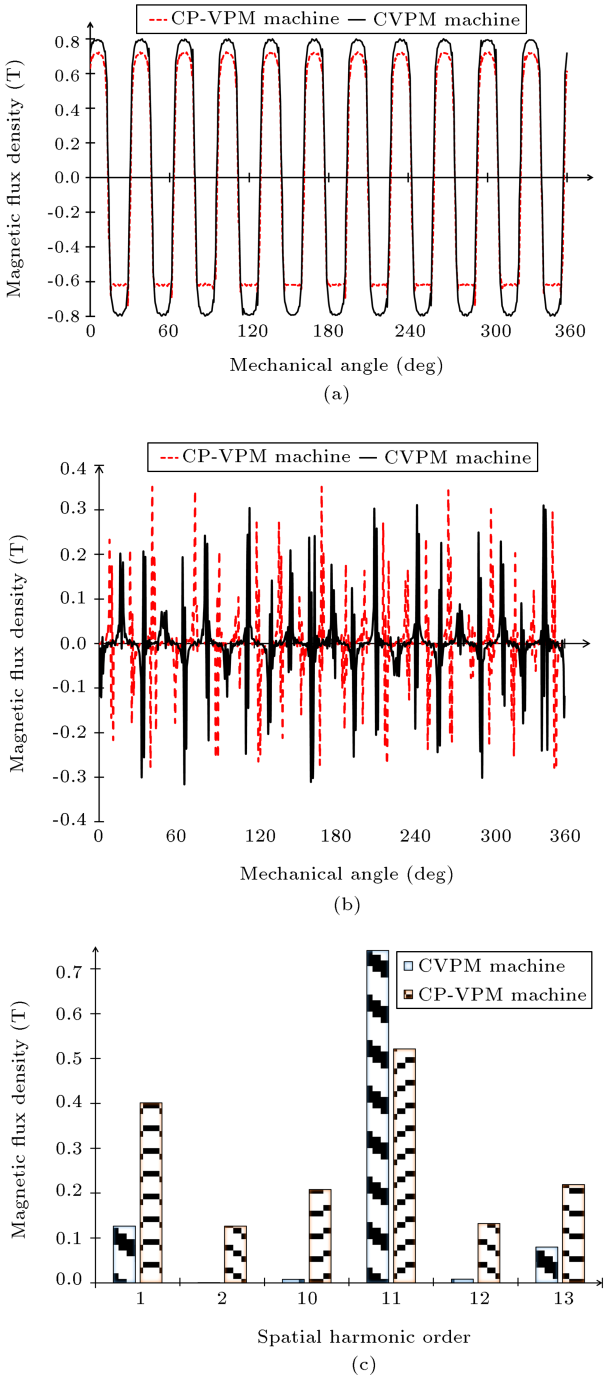

Figure 6. The air-gap magnetic field of the studied structures due to parallel magnetized PMs and considering slot-less stator core: (a) The spatial distributions of radial components, (b) the spatial distributions of tangential components, and (c) the dominant magnitudes with low order harmonics.

where B_{ag0} and B_{ag1} are expressed in Eqs. (12) and (13), respectively. Only these magnetic field components contribute to the developed torque and induced back EMF.

$$B_{ag0} = \Gamma_{PM1}\Lambda_{ag0}, \tag{12}$$

$$B_{ag1} = \Gamma_{PM1}\Lambda_{s1}/(2k_{cr}), \tag{13}$$

where Γ_{PM1} is the fundamental component of the PMs MMF distribution, i.e., $4\Gamma_{PM,\max}/\pi$.

In this relation, only the constant and fundamental terms of the stator and rotor permeance distributions and rotor MMF distribution are taken into account.

It can be concluded from the results that the induced back EMF has a much larger magnitude in the case of CP structure. The analytical expressions of the back EMF, output power, and power factor for VPM machine were derived from the reference study [15]. These relations are used to analytically compare the performances of the studied machines in Table 2, which are in good agreement with the FE results.

The electro-magnetic torque is also enhanced by almost 25%. However, the power factor is reduced severely. In general, the major drawback of the VPM machines is their low power factor, and improving the input power factor has been the main goal of several published papers such as [24]. For example, the dual-stator spoke-array VPM topology has been introduced to overcome the power-factor issue.

The leakage inductance of CP-VPM structure is higher than that of CVPM structure due to increased differential leakage term. Hence, proposing design modifications to enhance the power factor by reducing the undesirable spatial harmonics is pursued in the next section.

Table 2. Comparisons of the performance of the studied Conventional VPM (CVPM) and Consequent-Pole Vernier PM (CP-VPM) structures.

Characteristic	CVPM	CP-VPM
Back-EMF magnitude	175.1 V_{rms}	377.2 V_{rms}
Average torque	9.7 Nm	12.13 Nm
Power factor	0.73	0.46

The air-gap flux density distributions of both studied machines are depicted in Figure 7. As it can be seen, the air-gap flux density has a symmetrical waveform in the case of CVPM machine and an unbalanced distribution of CP-VPM machine due to spatial harmonic components with even orders. Hence, unbalanced magnetic force is created between stator and rotor bodies. In order to validate the derived analytical expressions, the values of the air-gap flux density components predicted using Eq. (11) are compared in Table 3 with the values obtained using 2D FE analyses. The maximum exposed error using the analytical equation is below 10%, which proves the accuracy of the analytical equations.

The back EMF and radial magnetic force waveforms, which are obtained from FE analyses, are shown in Figure 8. It should be noted that the radial forces in two halves of a conventional PM machine are in the opposite directions. Hence, no radial force acts on the machine bearings, theoretically. However, there is always unidirectional radial force in VPM machine bearings because of unequal numbers of stator poles and rotor magnets. This rotating unidirectional force is even larger by incorporating CP rotor due to the unbalanced distribution of magnetic field. The magnitude of net radial force on rotor body for the CVPM and CP-VPM studied machines is approximately 10 and 100 in Newton, respectively.

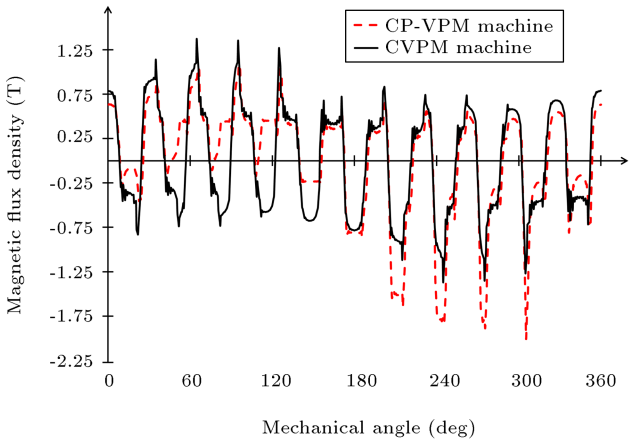

Figure 7. The air-gap flux density distributions of the studied Conventional VPM (CVPM) and Consequent-Pole Vernier PM (CP-VPM) machines.

Table 3. The magnitudes of the desired components of air-gap flux densities of the studied Conventional VPM (CVPM) and Consequent-Pole Vernier PM (CP-VPM) machines.

	Analytical method		2D-FE method	
	B_{ag0}	B_{ag1}	B_{ag0}	B_{ag1}
CVPM Machine	0.83 T	0.19 T	0.76 T	0.18 T
CP-VPM Machine	0.64 T	0.48 T	0.59 T	0.44 T

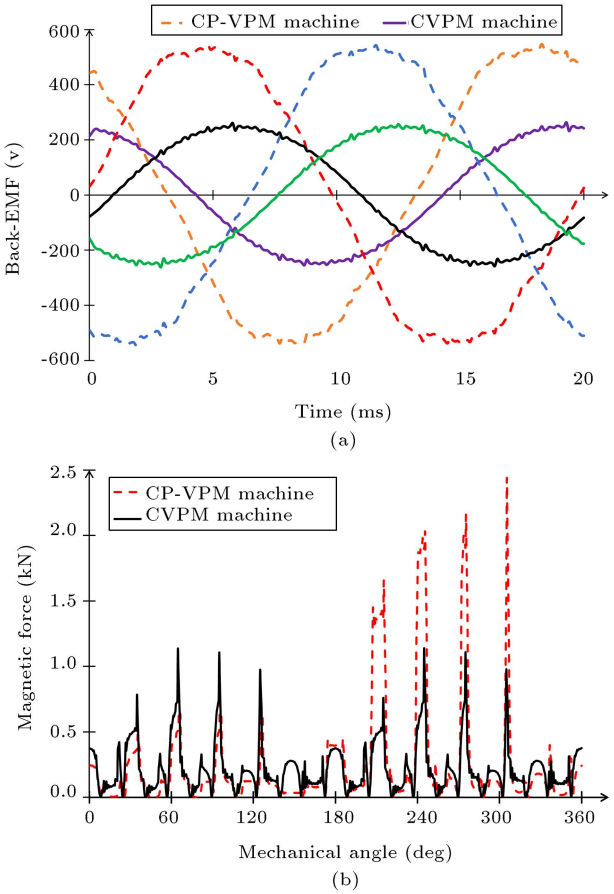

Figure 8. Comparison of the operating features of the machines with specifications given in Table 1: (a) Back EMF waveforms and (b) magnetic force waveforms.

3. Design modifications

The key factor in improving the power factor of CP-VPM machine is reduction of magnetic field spatial harmonic distortion. The peak value of Λ_{s1}, which maximizes the modulation flux, happens at $0.5 < w_{sso}/\tau_{ss} < 0.6$ interval (see Figure 3). However, choosing this ratio as 0.625, i.e., 1/1.6, leads to elimination of spatial harmonics with higher orders, according to Eq. (6). Thus, some of the undesirable spatial harmonics of the air-gap magnetic field are omitted and the differential leakage inductance will be reduced. In a similar manner, the non-fundamental spatial harmonic orders of rotor permeance function, i.e., kN_{rs} with $k \geq 2$, are canceled by choosing the ratio of w_{rs}/τ_{rs} as 0.625.

Furthermore, several dominant spatial harmonic components of the rotor field are created due to the MMF distribution of the magnets. This function consists of odd harmonic orders in the case of CVPM machine while odd and even orders are present in the rotor MMF distribution of CP-VPM machine. It is worthy to note that the unsymmetrical variations in magnets MMF function, which result from the absence

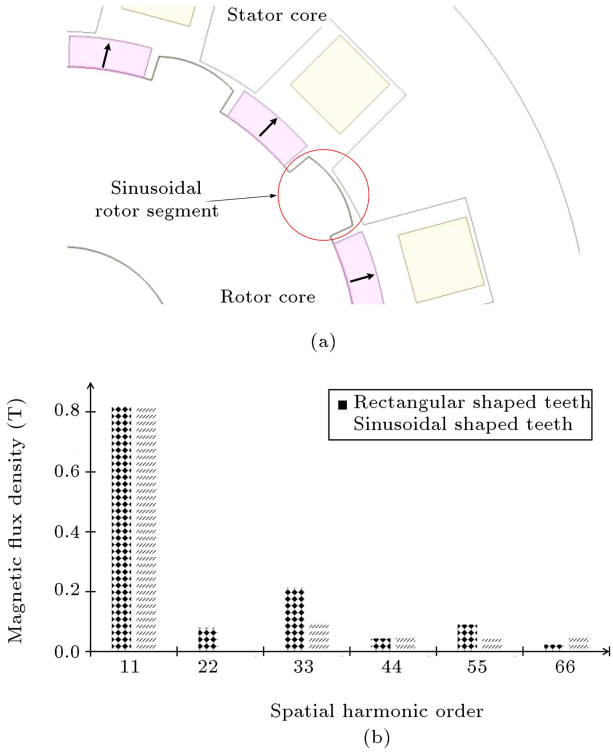

Figure 9. The CP rotor with sinusoidal teeth: (a) Geometrical view, (b) dominant rotor field spatial harmonics with rectangular and sinusoidal teeth.

of magnets with reverse magnetic polarization, lead to even spatial harmonic orders. The spatial harmonic distribution of the rotor magnetic field can be substantially improved by using sinusoidal rotor segments. The layout of the proposed rotor segments is shown in Figure 9(a). In this figure, the physical air-gap length is sinusoidally increased from 0.5 mm in the middle of rotor tooth up to 1.2 mm on tooth sides. The favorable effect of this geometrical modification is given in Figure 9(b), which shows the dominant spatial harmonic components of the rotor field considering rectangular and sinusoidal rotor teeth and slot-less stator core. Besides the benefit of reducing the differential leakage flux, the PM leakage flux is diminished due to increase of air-gap length at side ends of the teeth segments.

The third approach concerns the stator leakage inductance which is proportional to the square of the number of winding turns. According to the relations between back EMF and output power presented in [15], the winding conductors can be reduced in CP-VPM machine in order to develop the same torque density as the CVPM machine. This is because of its higher capability to produce the desirable component of rotor field through flux modulation. In this manner, the copper loss is diminished significantly, in addition to the improvement of the power-factor.

The effectiveness of the proposed modifications is studied in the next section using 2D-FE analyses.

4. Finite-element studies

The flux modulation capabilities of several VPM motors were compared using 2D-FE analyses. The cross-section of these machines is shown in Figure 10. It should be noted that the overall dimensions, the characteristics of the magnet and core materials, the stator specifications, and the excitation conditions are kept unchanged in all of the related studied structures. The results of average torque (T_{av}), cogging torque magnitude as a percentage of average torque (T_{cogg}), and the input Power-Factor are given in Figure 11(a) and the cogging torque waveforms are shown in Figure 11(b). The torque waveforms of Figure 11 are obtained using FE analyses in the fixed rotating speed condition. The windings are excited by current sources so that the resulted stator magnetic field is completely aligned with the rotating magnets field from the starting moment. Thus, no transient behavior is met and the results are in a steady-state condition from the start.

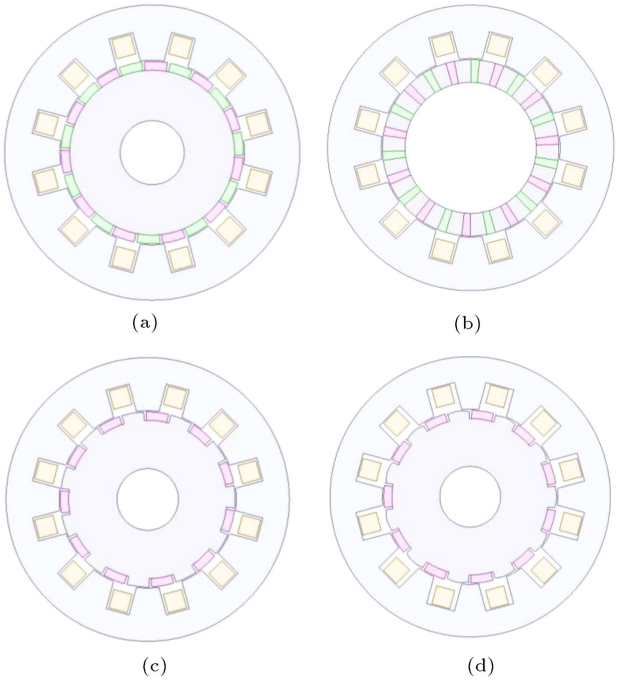

Figure 10. 2D cross-section of different PM vernier motors: (a) Conventional VPM (CVPM) motor, (b) spoke-array Vernier PM (VPM) motor, (c) Consequent-Pole Vernier PM (CP-VPM) motor with no design modifications, and (d) CP-VPM motor with modified stator and rotor teeth widths and sinusoidal rotor teeth.

The spoke-array VPM motor has the best power factor and the worst torque density and cogging torque portion. The torque density increased in the conventional surface-mounted VPM motor with the slight decrement of the power factor. Moreover, the torque ripples were reduced significantly. By using CP rotor topology, the average torque increased by almost 25% in comparison to the conventional topology. However, the variations in torque ripple magnitude, especially in power factor, are not satisfactory. These parameters were enhanced by changing the ratio of the slot opening width to the slot pitch length to 0.625 for stator and rotor slots. The torque waveform can be even smoother by changing the rectangular shaped rotor teeth into a sinusoidal shape. The enhancements were almost 34% and 50% for the average torque and torque ripple, respectively, while the power factor was lower by almost 26%.

In the following, the 2D-FE analyses demonstrate that the power-factor of the modified design structure can be enhanced to 0.68 by reducing the number of turns per coil from 200 (see Table 1) to 145. The resulted machine provides the average torque value of 9.8 Nm and the peak-peak cogging torque of 1.1%. Therefore, almost the same operating characteristics as the CVPM machine can be achieved using the CP-VPM machine by introducing interesting benefits of incorporating much lower magnet volume and producing lower copper loss and thus higher efficiency. Finally, according to related findings, optimizing design and proposing novel structures with enhanced performance besides the interesting features of the CP-VPM machine will facilitate upgrading its condition against the other possible types of direct-drive machines.

Table 4 presents the self and mutual inductance of the stator windings of the structures in Figure 10. It should be noted that the winding inductances are

Table 4. The self and mutual inductance of the stator windings of the structures presented in Figure 10.

Structure	Self inductance of stator winding	Mutual inductance between stator windings
Figure 10(a)	131.7 mH	–50.2 mH
Figure 10(b)	50.9 mH	–6.37 mH
Figure 10(c)	356 mH	–135.2 mH
Figure 10(c) with modified stator and rotor teeth widthes	308 mH	–118.4 mH
Figure 10(d)	260.4 mH	–101.1 mH

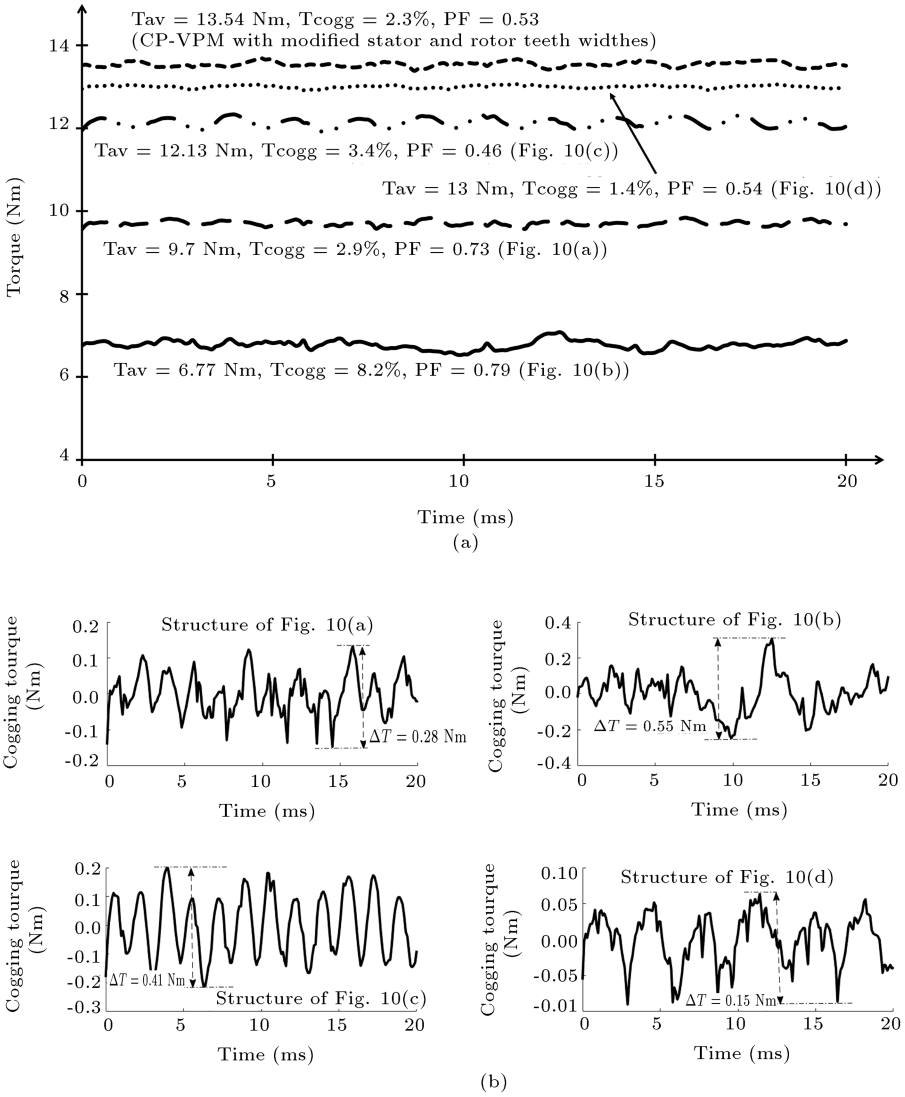

Figure 11. (a) The developed torque curves and (b) the cogging torque curves of Vernier PM (VPM) motors in Figure 10.

almost fixed values in CVPM machine. However, oscillations with low amplitudes are inserted on inductance waveforms of the other structures due to rotor saliency. The winding inductance of CVPM machine is lower than that of CP-VPM machine because of larger equivalent air-gap length. The inductance values vary in different CP-VPM structures with different stator and rotor teeth dimensions. Also, the spoke-array structure (Figure 10(b)) possess the lowest inductance with respect to its special rotor geometry with several PM segments in the magnetic flux route.

The back EMF and magnetic force waveforms of Figure 10(a) and (c) structures are illustrated in Figure 8. These waveforms for the structures in Figure 10(b) and (d) are shown in Figure 12. The same variations as the winding inductance values can be seen in the magnitudes of the induced back EMFs.

In order to validate the effectiveness of the proposed modifications, 3D-FE analyses of the final design, i.e., structure of Figure 10(d), are performed. In these studies, the magnitude of excitation current varied and the developed electro-magnetic torque and its pulsation magnitude are compared with 2D-FE analyses results. The exploded-view drawing of the simulated machine is shown in Figure 13 and the results of average and ripple torque magnitudes are compared in Figure 14(a) and (b), respectively. As it can be seen, the results are in good agreement and the exposed error is acceptable by omitting third dimension details, which keeps computational burden considerably low.

5. Conclusions

The paper presented the electro-magnetic operating principles of the consequent-pole Vernier PM machine using the analytical relations of the air-gap permeance

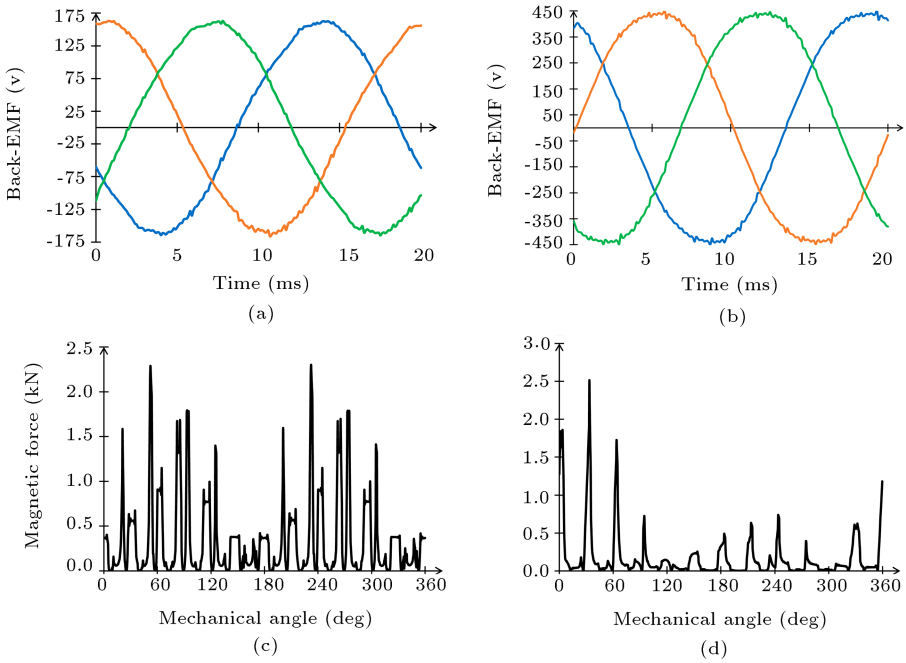

Figure 12. Back-EMF and magnetic force waveforms of the structures of Figure 10(b) and (d): (a) Back-EMF waveform of Figure 10(b) structure, (b) back-EMF waveform of Figure 10(d) structure, (c) magnetic force distribution in air-gap region of Figure 10(b) structure, and (d) magnetic force distribution in air-gap region of Figure 10(d) structure.

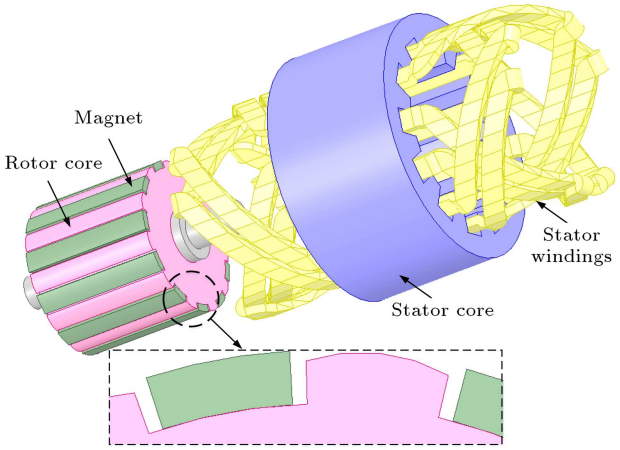

Figure 13. 3D exploded view of the final design with all the proposed modifications.

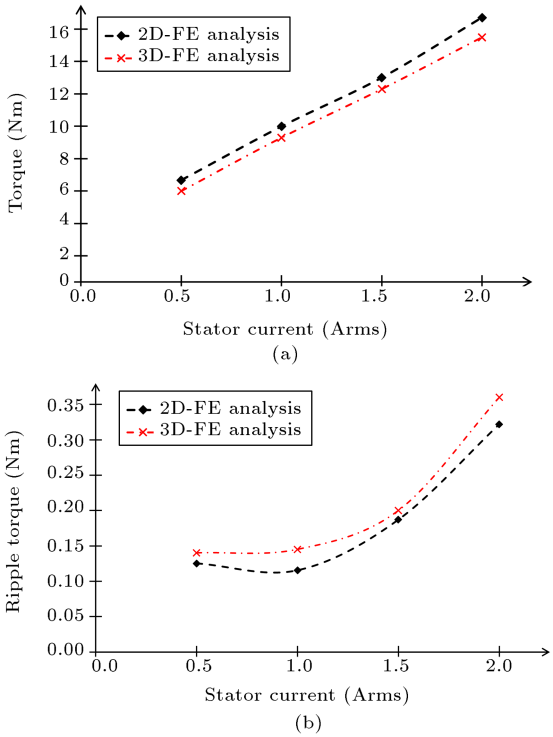

Figure 14. The results of 2D and 3D Finite Element (FE) analyses of structure of Figure 10(d): (a) Average electro-magnetic torque versus stator current, and (b) ripple torque magnitude versus stator current.

and MMF distributions. This particular Vernier PM topology requires a much lower PM material volume than the conventional Vernier PM or spoke-array structures, resulting in lower manufacturing cost. Although the axial and radial flux types of the conventional Vernier PM machines have been manufactured and incorporated in the electric and hybrid vehicles, the Consequent-Pole Vernier PM (CP-VPM) topologies are still in research stage. A comprehensive evaluation of the advantages and disadvantages of the CP-VPM and Conventional VPM (CVPM) machines was performed by studying the average and ripple torque magnitudes, the input power factor, and the unidirectional radial force. It was concluded that almost the same operating characteristics as the CVPM machine could be met using the CP-VPM machine. However, several interesting benefits make the CP-VPM machine a

suitable choice to be utilized in electric transportation vehicles and other low-speed and high-torque devices including incorporation of much lower PM material volume, smoother torque waveform, higher efficiency, and simpler and robust installation of PM pieces on the rotor surface.

References

1. Wu, Y.C. and Chen, Y.T. "Mitigation of cogging torque for brushless interior permanent-magnet motors", *Scientia Iranica*, **22**(6), pp. 2163–2169 (2015).
2. Abbaszadeh, K. and Rahimi, A. "Analytical quasi 3D modeling of an axial flux PM motor with static eccentricity fault", *Scientia Iranica*, **22**(6), pp. 2482–2491 (2015).
3. Du, Z.S. and Lipo, T.A. "Torque performance comparison between a ferrite magnet vernier motor and an industrial interior permanent magnet machine", *IEEE Transactions on Industry Applications*, **53**(3), pp. 2088–2097 (2017).
4. Wang, H., Fang, S., Yang, H., et al. "A Novel consequent-pole hybrid excited vernier machine", *IEEE Transactions on Magnetics*, **53**(11), pp. 1–4 (2017).
5. Ishizaki, A., Tanaka, T., Takasaki, K., et al. "Theory and optimum design of PM Vernier motor", *1995 Seventh International Conference on Electrical Machines and Drives (Conf. Publ. No. 412)*, Durham, UK, pp. 208–212 (1995).
6. Bai, J., Liu, J., Wang, M., et al. "Investigation of a less rare-earth permanent-magnet machine with the consequent pole rotor", *AIP Advances*, **8**(5), pp. 1–6 (2018).
7. Li, D., Qu, R., Li, J., et al. "Design of consequent pole, toroidal winding, outer rotor vernier permanent magnet machines", *2014 IEEE Energy Conversion Congress and Exposition (ECCE)*, Pittsburgh, PA, pp. 2342–2349 (2014).
8. Zhao, W., Zheng, J., Wang, J., et al. "Design and analysis of a linear permanent- magnet vernier machine With improved force density", *IEEE Transactions on Industrial Electronics*, **63**(4), pp. 2072–2082 (2016).
9. Zou, T., Li, D., Qu, R., et al. "Analysis of a dual-rotor, toroidal-winding, axial-flux vernier permanent magnet machine", *IEEE Transactions on Industry Applications*, **53**(3), pp. 1920–1930 (2017).
10. Zou, T., Li, D., Qu, R., et al. "Advanced high torque density PM vernier machine with multiple working harmonics", *IEEE Transactions on Industry Applications*, **53**(6), pp. 5295–5304 (2017).
11. Zhao, W., Chen, D., Lipo, T. A., et al. "Dual airgap stator- and rotor-permanent magnet machines with spoke-type configurations using phase-group concentrated coil windings", *IEEE Transactions on Industry Applications*, **53**(4), pp. 3327–3335 (2017).
12. Xu, L., Liu, G., Zhao, W., et al. "High-performance fault tolerant halbach permanent magnet vernier machines for safety-critical applications", *IEEE Transactions on Magnetics*, **52**(7), pp. 1–4 (2016).
13. Xie, K., Li, D., Qu, R., et al. "A novel permanent magnet vernier machine with halbach array magnets in stator slot opening", *IEEE Transactions on Magnetics*, **53**(6), pp. 1–5 (2017).
14. Zhu, X., Zhao, W., and Zhu, J. "A high power factor fault-tolerant vernier permanent-magnet machine", *AIP Advances*, **7**(5), pp. 1–4 (2017).
15. Kim, B. and Lipo, T.A. "Operation and design principles of a PM vernier motor", *IEEE Transactions on Industry Applications*, **50**(6), pp. 3656–3663 (2014).
16. Ho, S.L., Niu, S., and Fu, W.N. "Design and comparison of vernier permanent magnet machines", *IEEE Transactions on Magnetics*, **47**(10), pp. 3280–3283 (2011).
17. Li, D., Qu, R., Li, J., et al. "Analysis of torque capability and quality in vernier permanent-magnet machines", *IEEE Transactions on Industry Applications*, **52**(1), pp. 125–135 (2016).
18. Yang, Y., Liu, G., Yang, X., et al. "Analytical electromagnetic performance calculation of vernier hybrid permanent magnet machine", *IEEE Transactions on Magnetics*, **54**(6), pp. 1–12 (2018).
19. Kim, B. "Design of a PM vernier machine with consideration for modulation flux and comparison with conventional PM motors", *Energies*, **10**(11), pp. 1–12 (2017).
20. Okada, K., Niguchi, N., and Hirata, K. "Analysis of a vernier motor with concentrated windings", *IEEE Transactions on Magnetics*, **49**(5), pp. 2241–2244 (2013).
21. Liu, G., Jiang, S., Zhao, W., et al. "A new modeling approach for permanent magnet vernier machine with modulation effect consideration", *IEEE Transactions on Magnetics*, **53**(1), pp. 1–12 (2017).
22. Li, D., Qu, R., Li, J., et al. "Analysis of torque capability and quality in vernier permanent-magnet machines", *IEEE Transactions on Industry Applications*, **52**(1), pp. 125–135 (2016).
23. Heller, B. and Hamata, V., *Harmonics Field Effects in Induction Machines*, Elsevier Scientific Pub. (1977).
24. Li, D., Qu, R., and Lipo, T.A. "High-power-factor vernier permanent-magnet machines", *IEEE Transactions on Industry Applications*, **50**(6), pp. 3664–3674 (2014).

Biography

Hamed Gorginpour was born in Bushehr, Iran in 1985. He received the BSc degree in Electrical

Engineering from Shiraz University, Shiraz, Iran in 2007 and MSc and PhD degrees from Sharif University of Technology (SUT), Tehran, Iran in 2009 and 2014, respectively. He is currently an Assistant Professor at Persian Gulf University (PGU), Bushehr, Iran. His research interests include electrical machine design and modelling, finite element analysis, and power electronics and drives.